

# Seismic Vulnerability of Old Masonry Buildings – SEVERES Project

Jelena Milošević, Rita Bento, António Sousa Gago and Mário Lopes

## CONTENTS

<b>I</b>	<b>Numerical modeling</b>	4
<b>II</b>	<b>Diagonal Compression Tests</b>	4
II-A	Nonlinear Finite Element Model . . . . .	4
II-B	Distinct Element Model . . . . .	5
II-C	Discussion . . . . .	7
<b>III</b>	<b>Triplet Tests</b>	7
III-A	Nonlinear Finite Element Model . . . . .	7
III-B	Distinct Element Model . . . . .	8
III-C	Discussion . . . . .	9
	<b>References</b>	10

## LIST OF FIGURES

1	Finite element model mesh. . . . .	4
2	Numerical and experimental results: Force vs. Vertical displacement diagram for wall W4. . . . .	5
3	Numerical and experimental results: Force vs. Vertical displacement diagram for wall W2. . . . .	5
4	Randomly sized polygonal blocks. . . . .	5
5	Experimental and numerical failure modes: (a) Experimental; (b) Finite element model; (c) Distinct element model (the picture shows the wall immediately before the complete collapse) . . . . .	6
6	Experimental and numerical failure modes: (a) Experimental; (b) Finite element model; (c) Distinct element model (the picture shows the wall immediately before the complete collapse) . . . . .	6
7	Main crack obtained by the distinct element model - Wall W4. . . . .	6
8	Finite element model mesh. . . . .	7
9	Experimental and numerical failure modes: (a) Experimental; (b) Finite element model; (c) Distinct element model . . . . .	8
10	Experimental and numerical failure modes: (a) Experimental; (b) Finite element model; (c) Distinct element model . . . . .	8
11	Numerical and experimental results: Force vs. Horizontal displacement diagram for wall T3. . . . .	8
12	Numerical and experimental results: Force vs. Horizontal displacement diagram for wall T8. . . . .	9
13	Finite element triangular mesh. . . . .	9

## LIST OF TABLES

I	Mechanical properties for numerical analysis with finite element method . . . . .	6
II	Mechanical properties for numerical analysis with distinct element model . . . . .	7
III	Elastic properties for the continuum and interface elements . . . . .	9
IV	Inelastic properties for interface elements . . . . .	9
V	Mechanical properties adopted for the distinct element model . . . . .	10

# Seismic Vulnerability of Old Masonry Buildings – SEVERES Project

## I. NUMERICAL MODELING

Experimental tests provide values for mechanical parameters, but those values cannot be directly used in numerical modeling. A calibration process should be done in order to validate the values adopted for the mechanical parameters as well as the numerical models. This calibration process is extremely important when nonlinear material behavior is to be simulated, which is the case of seismic structural studies on old masonry buildings [2].

There is little information about old masonry buildings mechanical parameters, but even less with regard to its use in numerical models. In the present work two types of numerical models were built to simulate the diagonal compression tests described in report 1: nonlinear finite element models [3] and distinct element models [4].

In the finite element models the cracking of masonry (the most important source of non-linear behavior) was simulated by a smeared crack approach. In the case of rubble stone masonry walls, where the location of potential cracks cannot be defined in advance, a smeared model seems to be preferable and more applicable for engineering practice than a distinct crack approach. However, it should be noticed that when the complete material degradation is to be modeled, smeared crack models are more unstable than distinct crack models.

The distinct elements method was primary developed for rock mechanics, but its numerical robustness and its properties, namely in the simulation of the interaction between elements (or blocks), make the method very attractive for modeling masonry structures. The distinct element method allows the explicit modeling of stones and mortar joints, with displacements and rotations of the individual blocks, and, thus, the simulation of masonry walls failure mechanisms. The use of Voronoi algorithm [5] for elements (blocks) generation allowed reproducing the arbitrary stone arrangements in the masonry specimens and made possible the use of distinct element method for rubble stone masonry specimens.

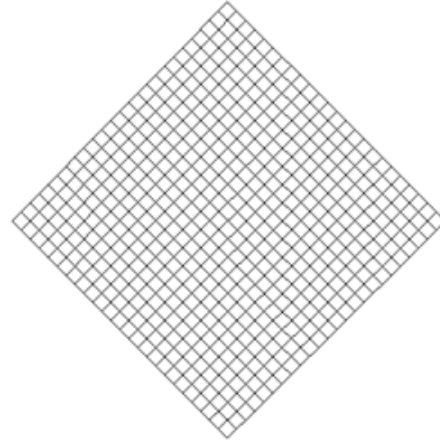


Fig. 1. Finite element model mesh.

## II. DIAGONAL COMPRESSION TESTS

### A. Nonlinear Finite Element Model

The adopted methodology for modeling the masonry specimens by the finite element method required the use of nonlinear models to simulate the masonry non tension resistance. A smeared crack model (Total Strain Crack Model [3]) based on a fixed stress-strain concept was used. In this model the stress-strain relations are evaluated in a fixed coordinate system which is fixed upon cracking. In others words, the crack orientation is kept constant during the whole computation process, which is physically realistic in the current case of study. Nonlinear geometric effects were not considered in the numerical simulations and eight-node isoparametric plane stress elements were used in the mesh generation (Figure 1).

The smeared crack models are defined through the combination of three factors: 1) a tension cut-off failure criterion (constant or linear), 2) the shear transfer through the crack (total, constant or variable shear retention) and 3) the material softening behavior (brittle, linear, multilinear or non-linear). In the present work a constant tension cut-off criteria was used together with an exponential constitutive law for the softening behavior. For the shear behavior it was adopted a constant shear retention (where the shear stiffness was reduced in the crack surface by 1% after cracking) and for the

compressive behavior an elastic linear constitutive law was used.

The finite elements mechanical properties for both type of specimens, namely the density  $\rho$ , Young modulus  $E$ , Poissons ratio  $\nu$ , tensile strength  $f_t$ , fracture energy  $G_{f1}$  and shear retention factor  $\beta$ , are presented in Table I. For density, Poissons ratio and fracture energy typical values adopted in other numerical works [[6], [7], [8], [9]] were considered.

For the shear retention factor, a parameter associated with the shear transference across cracks, the used value was obtained by calibration of the experimental and numerical results. The adopted value ( $\beta=0.1$ ) is a current value used in the simulation of the cracked plain concrete behavior, but slightly bigger than the value used by Rots et. al. [7] and [8]. However the adopted value is coherent with the experimental evidence where the stones interlock allow a important shear transference after crack occurrence.

The Young modulus and tensile strength were also quantified by calibration of the numerical and experimental results. With those results, which are not far from the typical values, a good match was obtained.

The vertical load was applied monotonically at the top of the specimen, as in the experiments, and a displacement controlled procedure was applied to impose the load up to failure, using the regular Newton-Raphson iteration procedure.

Considering the results obtained with the finite element method, that can be seen on Figure 2 and 3, an acceptable matching between numerical and experimental values for both the ultimate load and the initial loading branch are obtained. The damages observed in the numerical model are also coherent with the observed collapse during the experimental tests, as can be seen in Figures 5(a) and 5(b) for hydraulic lime mortar and Figure 6(a) and 6(b) for air lime mortar. Figure 2 and 3 also show the ultimate load obtained by the distinct element method referred later in the following part.

### B. Distinct Element Model

As mentioned, the distinct element models of the masonry specimens consisted in a group of randomly sized polygonal blocks generated by an automatic joint generator (Figure 4). Each block simulates a stone and was modeled by a finite difference elements mesh (Figure 4) with linear elastic behavior (bulk modulus  $K$  and shear modulus  $G$ ). In addition, an appropriate behavior was assigned to the contacts between the blocks using a Coulomb slip model. The parameters that control the contact behavior are the normal stiffness ( $J_{kn}$ ), the shear

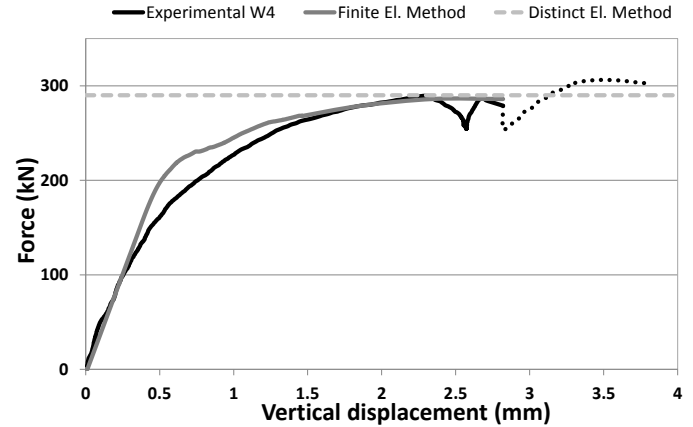


Fig. 2. Numerical and experimental results: Force vs. Vertical displacement diagram for wall W4.

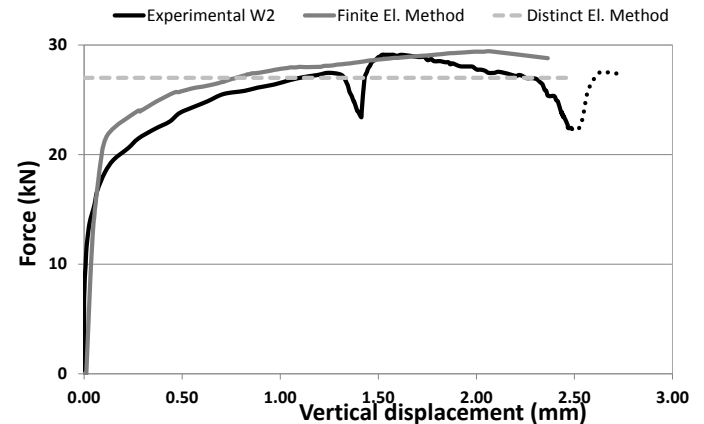


Fig. 3. Numerical and experimental results: Force vs. Vertical displacement diagram for wall W2.

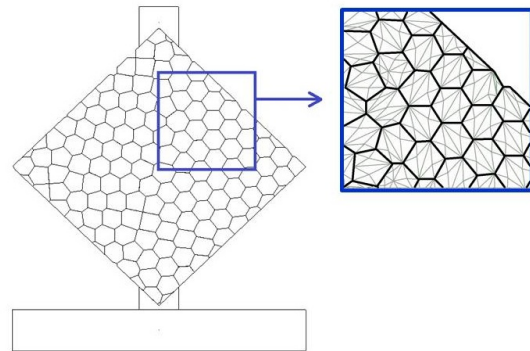


Fig. 4. Randomly sized polygonal blocks.

TABLE I  
MECHANICAL PROPERTIES FOR NUMERICAL ANALYSIS WITH FINITE ELEMENT METHOD

Masonry specimen	Density $\rho$ [kg/m <sup>3</sup> ]	Young modulus $E$ [GPa]	Poisson's ratio $\nu$	Tensile strength $f_t$ [MPa]	Fracture energy $G_{f1}$ [N/m]	Shear retention factor $\beta$
Hydraulic lime specimen	1835	3.27	0.20	0.15	100	0.1
Air lime specimen	1835	3.27	0.20	0.01	100	0.1

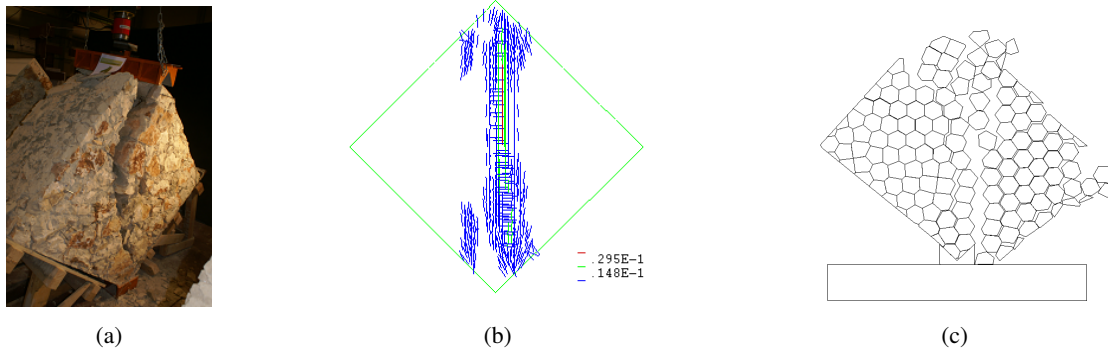


Fig. 5. Experimental and numerical failure modes: (a) Experimental; (b) Finite element model; (c) Distinct element model (the picture shows the wall immediately before the complete collapse)

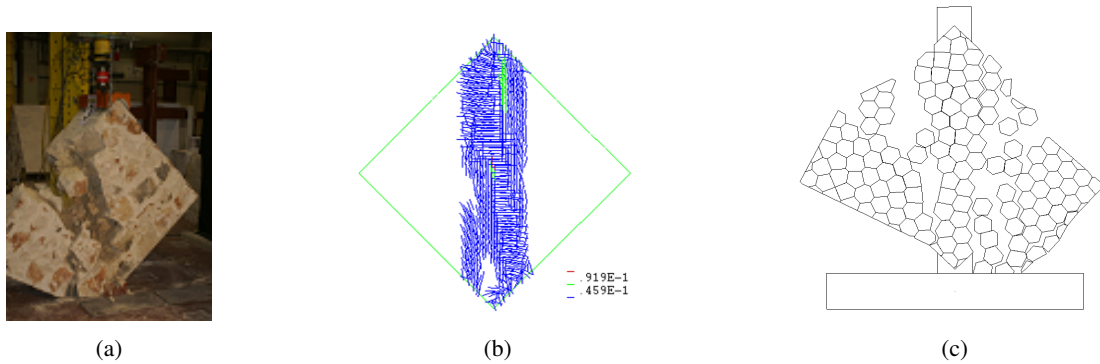


Fig. 6. Experimental and numerical failure modes: (a) Experimental; (b) Finite element model; (c) Distinct element model (the picture shows the wall immediately before the complete collapse)

stiffness ( $J_{ks}$ ), the friction angle ( $\phi$ ), the cohesion ( $c$ ) and the tensile strength ( $f_t$ ). The joint deformability parameters ( $J_{kn}$  and  $J_{ks}$ ) control the initial loading branch and the joint strength parameters ( $\phi$ ,  $c$  and  $f_t$ ) control the ultimate force level. The normal and shear stiffness are used to model the deformability of the mortar and blocks in the vicinity of the contact joint. Table II presents the adopted values for these parameters for the two cases: air lime mortar and hydraulic lime mortar specimens. Those values were quantified based on values adopted in other works [[9], [10], [11], [12]] and the calibration of the numerical and experimental results.

The numerical results obtained with the distinct element model for specimens made with hydraulic and air

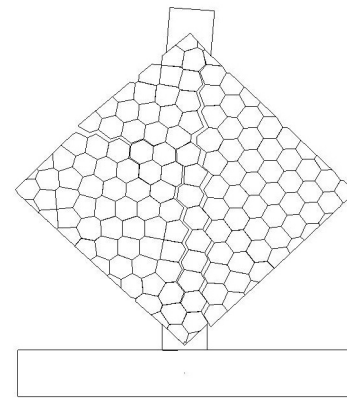


Fig. 7. Main crack obtained by the distinct element model - Wall W4.

TABLE II  
MECHANICAL PROPERTIES FOR NUMERICAL ANALYSIS WITH DISTINCT ELEMENT MODEL

Masonry specimen	Bulk modulus $K$ [MPa]	Shear modulus $G$ [MPa]	Normal stiffness $J_{kn}$ [GPa]	Shear stiffness $J_{ks}$ [GPa]	Friction angle $\phi$ [°]	Cohesion $c$ [MPa]	Tensile strength $f_t$ [MPa]
W4	410	450	17	17	45	0.23	0.23
W2	410	450	8	8	45	0.03	0.03

lime mortar can be seen in Figure 2 and 3, respectively, and the corresponding collapse mode for both type of mortar is depicted in Figure 5(c) and 6(c), respectively. In Figure 7 is depicted the main crack obtained on the distinct element simulations, which is similar to the crack observed in the experimental tests. As it can be seen in those figures a good matching between numerical and experimental values was achieved for the ultimate load and for the collapse pattern.

### C. Discussion

A general overview of the results obtained in numerical analysis was presented, where force displacement diagrams and failure modes were some of the aspects under analysis. An acceptable matching between numerical and experimental results for the ultimate load and collapse modes can be noted for both, finite element and distinct element models. As shown in Figure 5, 6 and 7, the obtained crack patterns (diagonal cracking) in the numerical models were quite similar to ones obtained in the experimental tests (Report 2). A good agreement with experimental results was also obtained in the finite element analysis for the initial branch of the load-displacement curve. In the distinct element analysis this curve cannot be obtained, at least not directly, which represents a clear advantage of the finite element method. However, modeling with finite element models was much more demanding in the sense that the numerical convergence required a continuous review of the convergence criteria. Since the location of the potential cracks are unknown in rubble stone masonry, the smeared crack approach is more appropriate for modeling large rubble stone masonry panels than the distinct crack approach or the distinct element method. However, the use of the Voronoi algorithm to randomly generate the blocks in the distinct element model allows the use of a distinct methodology in a smeared sense.

## III. TRIPLET TESTS

As for diagonal compression tests, two types of numerical models were used to simulate the triplet tests, namely a non-linear finite element model [3] and a distinct element model [4]. Both models are able to

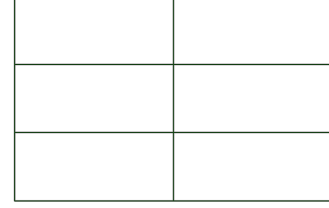


Fig. 8. Finite element model mesh.

simulate the masonry non-linear behavior, namely its shear strength and the reduced tensile strength.

In the finite element model a discrete approach was adopted. The three stone layers were modeled by nine-node continuum plane stress elements, while the mortar bed joints were simulated by six-node zero-thickness line interface elements. For the continuum elements a linear elastic behavior was adopted, being the non-linear behavior concentrated in the interface elements. The material model adopted for the interfaces was the multi-surface interface model proposed by Lourenço and Rots [13].

As already mention, the distinct element method allows the explicit modeling of stones and joints, with displacement and rotations of the individual blocks. In the experimental tests modeling each stone layer was model by an individual block, with linear elastic behavior (by triangular finite differences elements). As in the previous model, the non-linear behavior was concentrated in the joints, in this case by means of non-linear contacts.

### A. Nonlinear Finite Element Model

The multi-surface interface model proposed by Lourenço and Rots [13] is appropriate to simulate fracture, frictional slip as well as crushing along interfaces. The model assumes that the stone units behave in an elastic regime, while inelastic behavior is concentrated in the joints [3]. As mention, in the finite element model the stone layers were modeled using nine-node continuum plane stress elements, while the horizontal joints were represented by six-node zero-thickness line interface elements (Figure 8).

For the finite element model it was adopted the shear strength parameters obtained by the experimental tests

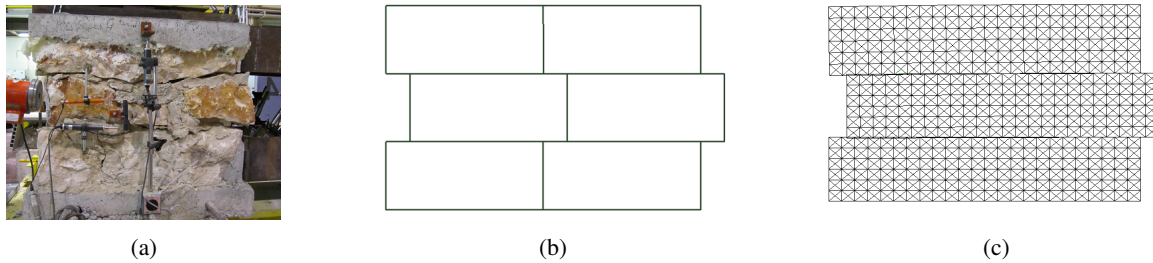


Fig. 9. Experimental and numerical failure modes: (a) Experimental; (b) Finite element model; (c) Distinct element model

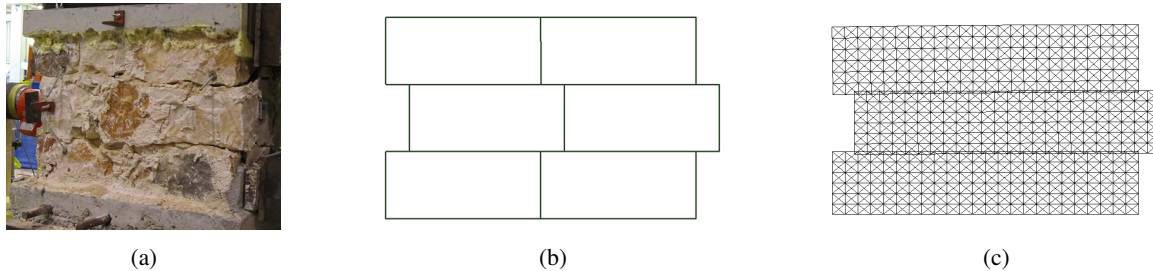


Fig. 10. Experimental and numerical failure modes: (a) Experimental; (b) Finite element model; (c) Distinct element model

(i.e. coefficient of friction ( $\tan \phi$ ) and cohesion ( $c$ )), as well as, the young modulus obtained experimentally for the vertical deformation of the stone layers. It must be mention that the for hydraulic lime and air lime mortar specimens it was found similar values for the young modulus, which means that the stones were in contact and the mortar hadnt an important influence in the deformability, at least in an early stage of vertical loading. The other interface parameters, like normal stiffness  $k_n$ , shear stiffness  $k_s$ , tensile strength  $f_t$ , fracture energies for Mode I ( $G_{(fI)}$ ) and Mode II ( $G_{(fII)}$ ), compressive fracture energy ( $G_{(fc)}$ ), dilatancy coefficient  $\tan \psi$ , and compressive strength  $f_c$ , were defined based on other works [[14], [15], [10]] and by trial and error, trying to adjust the numerical results to the experimental curves. Table III and Table IV summarize the elastic and inelastic parameters adopted for finite element models.

The boundary conditions and the load application were defined according to the experimental arrangement. Firstly the vertical load was applied in the upper surface and then the horizontal load was applied increasingly, till the specimen's collapse. The horizontal displacement of the right surfaces of the upper and lower stone layers were restricted, as happened in the experimental test. As can be seen in Figure 11 and Figure 12 the results obtained with the finite element method shows a reasonable matching between numerical and experimental values for both the ultimate load and the initial loading branch (Figure 11 and Figure 12 also show the ultimate load

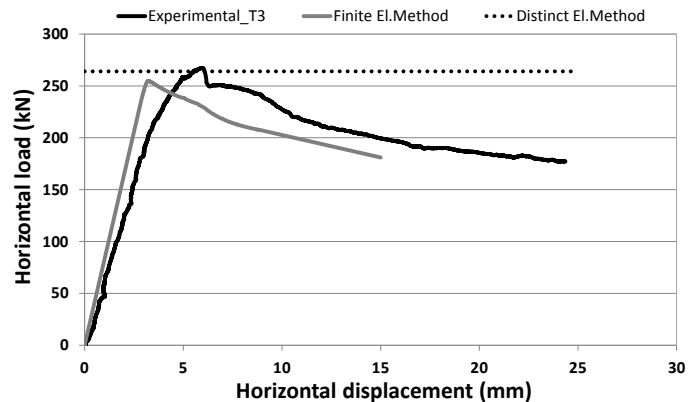


Fig. 11. Numerical and experimental results: Force vs. Horizontal displacement diagram for wall T3.

obtained by the distinct element method, referred later in the following part). Concerning the failure mode, the numerical models agreed reasonably well with the experimental evidence, as it can be noticed in Figures 9(a) and 9(b) for hydraulic mortar and Figure 10(a) and 10(b) for air lime mortar.

### B. Distinct Element Model

The distinct element model (Figure 13) consisted in a group of three blocks (each one simulating a stone layer and modeled by a finite difference elements mesh) with non-linear contacts between those block elements. For the finite difference triangular element mesh with

TABLE III  
ELASTIC PROPERTIES FOR THE CONTINUUM AND INTERFACE ELEMENTS

Mortar	Unit		Joint	
	$E$ [GPa]	$\nu$	$k_n$ [N/mm <sup>3</sup> ]	$k_s$ [N/mm <sup>3</sup> ]
Hydraulic	1.0	0.15	0.3	0.3
Air lime	1.0	0.15	0.07	0.07

TABLE IV  
INELASTIC PROPERTIES FOR INTERFACE ELEMENTS

Specimens	Tension		Shear				Compression	
	$f_t$ [MPa]	$G_{fI}$ [N/mm]	$c$ [MPa]	$\tan \phi$	$\tan \psi$	$G_{fII}$ [N/mm]	$f_c$ [GPa]	$G_{fc}$ [N/mm]
T3	0.1	0.1	0.2	1.23	0.001	0.5	5.0	5.0
T8	0.01	0.1	0.09	0.6	0.001	0.5	3.0	5.0

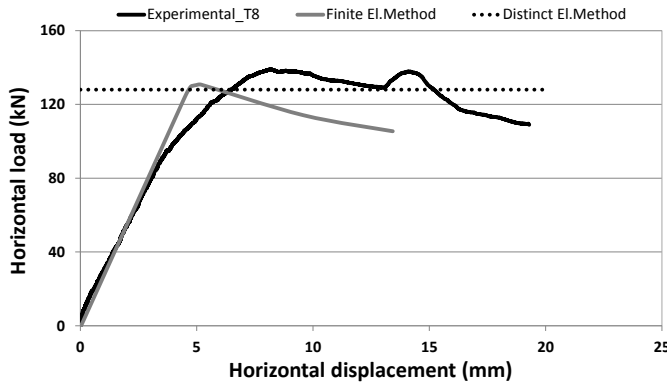


Fig. 12. Numerical and experimental results: Force vs. Horizontal displacement diagram for wall T8.

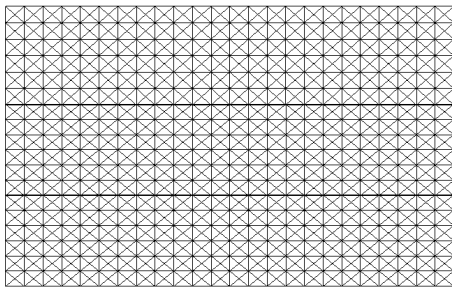


Fig. 13. Finite element triangular mesh.

linear elastic behavior it was adopted for the two types of specimens (hydraulic and air lime mortars) a bulk modulus ( $K$ ) of 480 MPa and a shear modulus ( $G$ ) of 430 MPa, which were obtained by a Young modulus ( $E$ ) of 1 GPa and a Poissons coefficient ( $\nu$ ) of 0.15.

An appropriate behavior was assigned for the contacts between blocks by a Coulomb slip model with residual

strength. The mechanical parameters of the mentioned contact model are the normal stiffness ( $J_{kn}$ ), the shear stiffness ( $J_{ks}$ ), the friction angle ( $\phi$ ), the residual friction angle ( $\phi_{res}$ ) the cohesion ( $c$ ), the residual cohesion ( $c_{res}$ ) and the tensile strength ( $f_t$ ) and the corresponding parameters for the residual strength. The joint deformability parameters ( $J_{kn}$  and  $J_{ks}$ ) control the initial loading branch and the joint strength parameters ( $\phi$ ,  $c$  and  $f_t$ ) control the ultimate force level. Those values were quantified considering the values obtained in the experimental tests (as in the finite element models) and by trial and error, trying to adjust the numerical and the experimental force-displacement curves. However, the trial and error procedure was based on values adopted in other works [[11], [16], [10]]. For the residual strength after the beginning of sliding, a degradation of 40% was estimated, based on the numerical and experimental results adjustment. Table V shows the adopted values for the contacts and blocks mechanical parameters.

As it can be seen in Figure 11 and Figure 12, for both type of wall specimens (hydraulic and air lime mortar) a good matching for the ultimate load was reached by the distinct element method. In the mentioned figures is presented only the maximum load obtained by the distinct element method, since for the software used the force-displacement curve can not be obtained, at least directly. Further developments should be done in the present work in order to obtain those curves. Finally, it worth mention that the models presented a failure pattern similar to the experimental one (Figure 9(c) and 10(c)).

### C. Discussion

As can be noticed, the numerical models (finite element and distinct element models), showed a good

TABLE V  
MECHANICAL PROPERTIES ADOPTED FOR THE DISTINCT ELEMENT MODEL

Masonry specimen	Bulk modulus $K$ [MPa]	Shear modulus $G$ [MPa]	Normal stiffness $J_{kn}$ [N/mm <sup>3</sup> ]	Shear stiffness $J_{ks}$ [N/mm <sup>3</sup> ]	Friction angle $\phi$ [°]	Residual friction angle $\phi_{res}$ [°]	Cohesion $c$ [MPa]	Residual cohesion $c_{res}$ [MPa]	Tensile strength $f_t$ [MPa]
T3	480	430	0.3	0.3	50	20	0.2	0.08	0.1
T8	480	430	0.07	0.07	30	12	0.09	0.036	0.01

matching between numerical and experimental results for the ultimate load and collapse modes. As can be seen in Figure 9 and 10 the obtained failure patterns (sliding) in the numerical models were quite similar to ones seen on the experimental tests. In the finite element analysis a good agreement with the experimental results was obtained for the initial branch of the "load-displacement" curve, which indicates that the elastic parameters were well estimated. Regarding the simulation of shear behavior after the maximum load, which required very small loading steps to get convergence in all steps, a good agreement was also obtained. That agreement was obtained mainly due to the values adopted for the Mode I and Mode II fracture energies, since the compressive strength and corresponding fracture energy were not relevant. The effect of dilatancy was not considered in the present finite element simulation, which requires further developments to understand its influence in the shear strength. In the distinct element analysis the force-displacement curve cannot be directly obtained, which represents an advantage of the finite element method. However, modeling with finite element models was much more demanding in the sense that the numerical convergence required a continuous review of the convergence criteria. For the contact behavior after the sliding, a residual strength of 40% was considered. That assumption, which as a similar effect to the fractures energies considered in the finite element models, must be confirmed in further developments of the present study by the complete force-displacement curve. Also in the distinct element model the effect of the dilatancy should be study in further developments of the present study.

## REFERENCES

- [1] Master's thesis.
- [2] P. B. Lourenço, P.B., "Computations on historic masonry structures," *Progress in Structural Engineering and Materials*, vol. 4, no. 3, pp. 301–319, 2002. [Online]. Available: <http://dx.doi.org/10.1002/pse.120>
- [3] DIANA, "DISplacement method ANALyser, release 9.1," *TNO DIANA BV*, 2005.
- [4] ITASCA, "UDEC version 4.01 - Users guide," *Itasca Consulting Group, Inc., Minneapolis, USA*, 2005.
- [5] K. R., "Concrete and Abstract Voronoi Diagrams," *Lecture Notes in Computer Science. 200. Springer-Verlag*, 1989.
- [6] N. Mendes and P. Lourenço, "Seismic Assessment of Masonry Gaioleiro Buildings in Lisbon, Portugal," *Journal of Earthquake Engineering*, vol. 14:1, pp. 80–101, 2010.
- [7] J. Rots, B. Belletti, M. Boonpichetvong, and S. Invernizzi, "Event by Event Strategies for Modeling Amsterdam Masonry Structures," in *Structural Analysis of Historical Constructions, New Delhi*, 2006.
- [8] L. Ramos and P. Lourenço, "Advanced numerical analysis of historical centers: A case study in Lisbon," *Engineering Structures* 26, pp. 1295–1310, 2004.
- [9] A. Gago, "Análise Estrutural de Arcos, Abóbadas e Cúpulas Contributo para o estudo do património construído (in portuguese)," Ph.D. dissertation, Faculty of Engineering, IST-UTL Technical University of Lisbon, 2004.
- [10] A. Gago, J. Alfaiate, and A. Lamas, "The effect of the infill in arched structures: Analytical and numerical modeling," *Engineering Structures* 33-5, pp. 1450–1458, 2011.
- [11] J. Azevedo, G. Sincaian, and J. V. Lemos, "Seismic behavior of blocky masonry structures," *Earthquake Spectra* 16-2, pp. 337–365, 2000.
- [12] J. Lemos, "Discrete element modelling of the seismic behaviour of stone masonry arches," *Computer Methods in Structural Masonry, London*, pp. 220–227, 1998.
- [13] P. Lourenço and J. Rots, "A multi-surface interface model for the analysis of masonry structures," *Journal of Eng. Mechanics, ASCE*, pp. 660–668, 1997.
- [14] R. Senthivel, P. Lourenço, and J. Rots, "Finite element modeling of deformation characteristic of historical stone masonry shear walls," *Journal of Eng. Structures*, pp. 1930–1943, 2009.
- [15] D. V. C. Oliveira, "Experimental and numerical analysis of blocky masonry structures under cyclic loading," Ph.D. dissertation, University of Minho, Portugal, 2003.
- [16] J. Lemos, "Discrete element modeling of masonry structures," *International Journal of Architectural Heritage: Conservation, Analysis, and Restoration*, pp. 190–213, 2007.